β-Lactamase of *Mycobacterium tuberculosis* shows dynamics in the active site that increase upon inhibitor binding

Running title: Dynamics of BlaC

Wouter Elings[a], Anamika Gaur[a], Anneloes J. Blok[a], Monika Timmer[a], Hugo van Ingen[a,b], Marcellus Ubbink[a,#]

[a] Leiden Institute of Chemistry, Leiden University, Einsteinweg 55, 2333 CC Leiden, The Netherlands

[b] Current address: Bijvoet Center for Biomolecular Research, Utrecht University, Padualaan 8, 3584 CH Utrecht, The Netherlands

[#] E-mail: m.ubbink@chem.leidenuniv.nl; phone: +31 71 5274628.

ABSTRACT: The *Mycobacterium tuberculosis* β-lactamase BlaC is a broad-spectrum β-lactamase that can convert a range of β-lactam antibiotics. Enzymes with low specificity are expected to exhibit active site flexibility. To probe the motions in BlaC, we studied the dynamic behavior in solution using NMR spectroscopy. ^{15}N relaxation experiments show that BlaC is mostly rigid on the pico- to nanosecond time scale. Saturation transfer experiments indicate that also on the high millisecond time scale BlaC is not dynamic. Using relaxation dispersion experiments, clear evidence was obtained for dynamics in the low millisecond range, with an exchange rate of *ca.* 860 s^{-1}. The dynamic amide groups are localized in the active site. Upon formation of an adduct with the inhibitor avibactam, extensive line broadening occurs, indicating an increase in magnitude of the active site dynamics. Furthermore, the rate of the motions increases significantly. Upon reaction with the inhibitor clavulanic acid, similar line broadening is accompanied by duplication of NMR signals, indicative of at least one additional, slower exchange

process (k_{ex} < 100 s^{-1}), while for this inhibitor also loss of pico- to nanosecond time scale rigidity is observed for some amides in the α-domain. Possible sources of the observed dynamics, such as motions in the omega loop and rearrangements of active site residues, are discussed. The increase in dynamics upon ligand binding argues against a model of inhibitor binding through conformational selection. Rather, the induced dynamics may serve to maximize the likelihood of sampling the optimal conformation for hydrolysis of the bound ligand.

KEYWORDS

BlaC, clavulanic acid, avibactam, NMR spectroscopy, inhibition, chemical exchange

INTRODUCTION

A central question in chemical biology is how enzymes can have broad specificity. Enzyme catalysis depends on efficient binding of the substrate to the enzyme and on the precise positioning of active site residues to stabilize the transition state. Substrates that are structurally diverse may require different active site conformations to efficiently bind the substrates and stabilize their respective transition states.(1–10) Consequently, a trade-off between active site rigidity for precise positioning of amino acid sidechains and flexibility for adaptation to various substrates will exist, requiring motions of parts of the enzyme. Protein motions can occur on a broad range of time scales. It has been hypothesized that enzymes that combine high catalytic efficiency with broad specificity, do so by combining high rigidity on short time scales with flexibility on longer time scales.(11) The dynamic behavior of Ambler class A β-lactamases TEM-1 and PSE-4 is in line with this idea (e.g. (11–16)). A combination of NMR backbone dynamics studies and molecular dynamics (MD) simulations has revealed that these proteins are extraordinarily rigid on the pico-nanosecond timescale, and display microsecond to millisecond timescale motions in the vicinity of the active site, in particular in the Ω-loop that encloses it on one side (Figure 1). Dynamics experiments on proposed β-lactamase ancestors(17–19) and chimera proteins(20,

21) suggested that this pattern of dynamics is a conserved feature. However, significant dynamic differences were found for individual residues, emphasizing the importance of comparing various β-lactamases.(15, 22) The leading structural model to explain the active site dynamics is a slow motion of the Ω-loop into and out of the active site. This loop contains residue Glu166, which acts as a general base for deacylation, activating a conserved water molecule for nucleophilic attack of the Ser70-bound carbonyl, which leads to hydrolysis of the bond between enzyme and adduct. Glu166 is also thought to play a similar role in acylation, although Lys73 has alternatively been proposed as general base for this step.(23, 24) Furthermore, other residues in the Ω-loop, such as Asn170, also contribute favorable enzyme-substrate interactions. These interactions may require slightly different enzyme conformations with various substrates. If active site flexibility is indeed required for adaptation to various substrates, it can be hypothesized that ligand binding will lock the active site in one conformation and thus freeze out the dynamics. NMR dynamics studies on β-lactamase / ligand complexes have not been reported to date, although the potential relevance of insight into the bound state dynamics has been recognized for years.(15) The absence of such data may be due to technical difficulties, as the typical length of NMR dynamics experiments is several days, restricting such studies to extremely stable complexes. Clearly, monitoring the dynamics during normal catalysis of substrates in this way is not feasible. However, β-lactamases do form stable covalent complexes with inhibitors. Inhibition of β-lactamases has clinical application(25–27) and is gaining in relevance with the increased prevalence of antibiotic resistance.(28–30) In addition to this inherent interest in β-lactamase inhibition, inhibitor-bound β-lactamases may also serve as a mimic of the covalent β-lactamase substrate complex during catalysis. We recently characterized the timescale of interaction between the β-lactamase of *Mycobacterium tuberculosis*, BlaC (Figure 1), and the inhibitor clavulanic acid in different buffers.(31) The high stability of the complex in MES buffer opens up a window for NMR dynamics measurements. Also the effects of the inhibitor avibactam, which binds reversibly rather than being degraded,(32) can be measured using these techniques.

Here, we present the dynamic properties of BlaC and the first characterization of β-lactamase / inhibitor complex dynamics. The dynamic behavior of resting state BlaC in solution is very similar to that of other class A β-lactamases and the rate of the active site exchange process is *ca.* 860 s^{-1} at 298 K. The high rigidity, which is a hallmark of β-lactamases, is locally lost upon inhibition by clavulanic acid. Furthermore, upon binding to either clavulanic acid or avibactam, the effects of chemical exchange in the active site become more extensive, clearly showing that inhibitor binding does not lock the active site in one conformation.

MATERIALS AND METHODS

Materials.

Pure BlaC without signal peptide and purification tag (sequence detailed in Figure S1) was obtained as described previously.(31) The Ambler standard β-lactamase numbering scheme (Figure S1) is used throughout this text.(33) Clavulanic acid from manufacturer Matrix Scientific was used, concentrations were determined using the previously determined extinction coefficient at 256 nm of 20.0 (0.1) mM^{-1} cm^{-1}.(31) Avibactam was used from manufacturer MedChem Express, concentration was determined using 1D ^{1}H quantitative NMR with TSP as a known standard.

Methods.

Unless mentioned otherwise, all experiments were performed on samples containing 0.38 mM ^{15}N enriched BlaC in 94 mM MES/NaOH pH 6.4 and 6 % D_2O, at 298 K. Measurements of inhibitor-bound BlaC were performed on samples obtained by mixing BlaC with the inhibitor in the same buffer, to concentrations after mixing of 0.38 mM BlaC and either 100 mM clavulanic acid or 2 mM avibactam, unless mentioned otherwise. NMR spectra were recorded on a Bruker AVIII HD 850 MHz (20 T) or Bruker AVIII 600 MHz (14 T) spectrometer equipped with a TCI cryoprobe or a TXI probe, respectively. ^{1}H, ^{15}N transverse relaxation optimized heteronuclear single quantum coherence (TROSY-HSQC)(34, 35) spectra were recorded and assigned using HNCa spectra on samples containing 0.7, 0.4 or 0.3 mM ^{15}N, ^{13}C enriched BlaC without inhibitor, with 186 mM clavulanic acid or with 2 mM

avibactam, respectively, in the same buffer. These spectra were recorded using standard Bruker pulse program 'trhncaetgp3d', processed with Topspin 3.2 (Bruker Biospin) and analyzed using CCPNmr Analysis.(36) Assignment was performed by comparison of the TROSY-HSQC and HNCa spectra with those of the previously assigned BlaC with a 6×His purification tag (Biological Magnetic Resonance Bank (BMRB) ID 27067).(31) Nuclear Overhauser effect (*NOE*) measurements were performed using standard Bruker pulse program 'hsqcnoef3gpsi', with a ^{1}H saturation delay of 4 s. ^{15}N longitudinal relaxation time (T_1) measurements were performed using standard Bruker pulse program 'hsqct1etf3gpsitc3d', with a recycle delay between experiments of 6 s and variable delays of 0.12, 0.17, 0.24 (2x), 0.33, 0.46, 0.65, 0.91, 1.28 (2x), 1.78 and 2.50 s. ^{15}N transverse relaxation time (T_2) measurements were performed using standard Bruker pulse program 'hsqct2etf3gpsitc3d', with a recycle delay between experiments of 4 s and 500 Hz CPMG refocusing strength during variable T_2-delays of *ca.* 0, 17, 34 (2x), 51, 68, 85, 102, 119 (2x), 136 and 153 ms. All relaxation experiments were acquired in an interleaved manner. T_1 and T_2 data were processed with Topspin 3.2 and resulting peak heights were fitted to exponential decay curves using Dynamics Center 2.5 (Bruker BioSpin). *NOE* data were processed and analyzed with the same software.

Lipari-Szabo analysis was performed with Dynamics Center 2.5. Only residues for which the *NOE* > 0.75 and the T_1 and T_2 values were each within one standard deviation of their respective means were used to fit the diffusion tensor. The diffusion was found to be anisotropic, with average rotational correlation time $\tau_c = 1 / (2 \times (D_{xx} + D_{yy} + D_{zz}))$(37) in line with a prediction from subunit A of crystal structure 5NJ2, after deletion of the histidine tag and linker, using HydroNMR(38). Least-squares fitting of the reduced spectral density function, $j(\omega)$, to the relaxation parameters was performed with 1000 iterations with random starting parameters, using an NH bond length of 1.02 Å and an average chemical shift anisotropy of -160 ppm. To avoid overfitting of relaxation parameters with small errors, Lipari-Szabo analyses were performed with user-defined errors of 10 % (T_1) and 5 % (T_2 and *NOE*) of the respective values. Relaxation data from each residue were fitted with the five standard models for internal motions, using anisotropic overall motion.(39, 40) In Model 1, the order parameter S^2 is fitted

for each residue, while the correlation times τ_j are calculated from components and orientation of the diffusion tensor, which is a global parameter. In Model 2, a local correlation time τ_e for fast motion is additionally fitted individually for each residue. Model 3 is the same as Model 1, except that an R_{ex} term is added to the R_2 in the calculation of the reduced spectral densities. Likewise, Model 4 is the same as Model 2 with the addition of an R_{ex} term. In Model 5, an extra modelling parameter S_f^2 is included for very fast local motion. The best model was selected based on the lowest *AIC* value, which is the sum of the χ^2 of the fit and the number of fitted parameters × 2. The selected model for each residue is reported with the relaxation data at BMRB (*vide supra*).

CPMG relaxation dispersion measurements were performed on 1.0, 0.8 or 0.4 mM ^{15}N enriched BlaC samples, for free protein at 20 T, at 14 T or with 100 mM inhibitor at 20 T, respectively. The TROSY CPMG pulse program as detailed by Vallurupalli *et al.*(41) was used, with two blocks of 1 (2x), 2, 3 (2x), 4, 6, 8, 10 (2x), 14, 18, 22, 28, 34 and 40 ^{15}N 180° pulses in 40 ms relaxation time, respectively. The length of the CPMG refocusing pulse was 84 µs and the carrier was set to the center of the spectrum at 119 ppm. Data were acquired in interleaved manner with a recycle delay of 2 s. Data were processed with NMRPipe(42) and resulting resonances were fitted to a glore line shape using FuDa.(43) Effective transverse relaxation rates $R_{2,eff}$ were calculated from the fitted peak heights using $R_{2,eff}(\nu_{CPMG}) = -ln(I(\nu_{CPMG}) / I_0) / T_{ex}$. In the relaxation dispersion data of BlaC bound to clavulanic acid, 29 of the 208 fitted profiles showed variations that were much bigger than the experimental noise. This variation is likely due to technical imperfections, so these data points were excluded from further analysis. An exclusion cut-off of 10 s^{-1} total increase in $R_{2,eff}$ between subsequent pulse frequencies was used. Chemical exchange rates were determined with a grouped fit with the software CATIA,(44) using a minimum $R_{2,eff}$ standard deviation of 0.8 s^{-1} to avoid over-fitting.

Chemical exchange saturation transfer (CEST) measurements were performed on 0.8 mM ^{15}N BlaC samples, using the standard Bruker 'hsqc_cest_etf3gpsitc3d' pulse program, with 2.5 s recycle delay and 0.8 s B_1 irradiation at 8 and 25 Hz at frequencies in the ^{15}N range 100.5:0.5:130 ppm.

Titration of BlaC with avibactam was performed by adding a solution of 6 mM avibactam in 94 mM MES/NaOH pH 6.4 and 6 % D_2O to a sample of 0.27 mM ^{15}N enriched BlaC in the same buffer, to concentrations of 0, 0.02, 0.07, 0.1, 0.2, 0.3, 0.4, 0.6, 0.7 and 0.9 mM avibactam. The final protein concentration was 0.23 mM. Affinity and off-rate were determined by fitting the peak shapes of Cys69, Arg161, Leu162, Glu168, Tyr241 and Ala274 over the course of the titration to a two-state binding model in TITAN.(45) The resulting standard deviations of the fitted K_D and k_{off} were unrealistically small, even after bootstrapping with 100 replicas, so the values are reported as an estimated confidence interval based on systematic variation of the parameters (Figure S2).

Figures containing the protein structure were created using the PyMOL Molecular Graphics System, Version 2.2 Schrödinger, LLC.

Data availability.

NMR chemical shift assignments and relaxation data have been submitted to the BMRB and can be accessed under BMRB IDs 27888 (free state), 27890 (clavulanic acid adduct-bound state) and 27929 (avibactam-bound state).

RESULTS

Resting state BlaC.

The ^{1}H, ^{15}N correlation spectra of BlaC are well dispersed (Figure S3). The backbone amide assignment of resting state BlaC without tag was derived from the previously published assignment of the tagged protein(31) via comparison with an HNCa spectrum. In this way, 98% of the resonances of the BlaC backbone H−N moieties could be assigned. As with the tagged protein, the four residues at hydrogen-bonding distance from the active site phosphate were the only nonproline, nonterminal residues for which backbone resonances could not be found. The four missing resonances, as well as the lower peak intensities of the surrounding amides (Figure 2a, black squares), suggest that an intermediate-to-fast exchange process may be present in the active site.

To characterize the dynamics processes, the ^{15}N longitudinal relaxation time (T_1), ^{15}N transverse relaxation time (T_2) and the ^{15}N-{^{1}H} nuclear Overhauser effect (*NOE*) of the BlaC backbone amides were measured at two magnetic fields, 14 T and 20 T (Figures S4 and S5). The obtained *NOE* ratios show lower values for loop and surface regions of the protein as well as an unexpectedly low ratio for Val80 (Figure S4), but overall BlaC is clearly a rigid protein on the pico-nanosecond time scale. Lipari-Szabo model-free analysis of the two-field T_1, T_2 and *NOE* data was performed using an anisotropic diffusion tensor, yielding an average rotational correlation time of 13.81 ± 0.04 ns. This is in agreement with an estimate using HydroNMR(38) and crystal structure 5NJ2(31) (14.5 ns). Fitting of the spectral densities resulted in an average order parameter over 0.9 and yielded very few dynamic regions, confirming that BlaC is rigid on the short time scales (Figure S6). Most amides were best fitted with anisotropic models 1-4 (see Materials and Methods). Only for Val80, model 5, including an extra local order parameter S_f^2 for very fast motion, was used to fit the data. The resulting order parameters are S_f^2 = 0.79 ± 0.03 and S^2 = 0.57 ± 0.02, the latter of which is the lowest order parameter in the protein. The other regions that exhibit some flexibility correspond with elements that are expected to be flexible based on the structure, such as the loop between β-strands 1 and 2 and that between α-helices 7 and 8.

Several residues could not be modelled without the inclusion of a chemical exchange parameter, so the possibility of exchange on the millisecond time scale was examined using CPMG relaxation dispersion measurements at magnetic field strengths of 14 T and 20 T. Dispersion of relaxation rates over the CPMG pulse frequency, indicating millisecond chemical exchange, was observed centered clearly around the active site (Figure 3 *(a)* and *(c)*, spheres in orange).

Eight active site residues that showed similar dispersion profiles at both magnetic field strengths were used in a group fit (Figures 4 and S7) yielding a chemical exchange rate of (8.6 ± 0.6) × 10^2 s^{-1}. This exchange rate agrees with the (8.5 ± 2.1) × 10^2 s^{-1} that was found for TEM-1 with single-field relaxation dispersion.(21) The excited state population and chemical shift differences could not be determined with any accuracy.

Antimicrobial Agents and Chemotherapy

196 To investigate the possibility of even slower dynamic processes, chemical exchange saturation transfer
197 (CEST) in resting state BlaC was also measured. Experiments with saturation fields of 25 Hz and 8 Hz
198 and at temperatures of 298 K and 288 K all failed to reveal chemical exchange for any of the residues,
199 suggesting that no significant dynamics in the CEST time scale of 20 - 200 s^{-1} are present. An example
200 profile is provided in Figure S8.
201

202 **Inhibitor-bound BlaC.**

203 The effect of BlaC inhibition on its dynamic behavior was studied by performing NMR experiments
204 on 0.38 mM BlaC with 2 mM avibactam or 100 mM clavulanic acid. Avibactam is not hydrolyzed by
205 BlaC, as was observed by others(32, 46) and also in our experiments (not shown). Clavulanate has a
206 ~1.2 h turnover time under these conditions,(31) so this large excess of clavulanic acid allowed the
207 recording of multidimensional NMR experiments on the BlaC/inhibitor complex. This turnover rate is
208 much too slow to affect the employed NMR dynamics experiments. Furthermore, the rate is much
209 slower than the other catalytic steps, so the adduct accumulates to a fraction close to 100%. Previously,
210 this major species was shown by mass spectrometry to be a 70 Da covalent adduct.(31) Thus, the NMR
211 dynamics measurements report on conformational dynamics of this major species. The ^{1}H-^{15}N TROSY-
212 HSQC spectra of backbone amides of BlaC bound to each inhibitor were assigned by comparison to the
213 spectra of resting state BlaC, with additional help of HNCa spectra of ^{15}N, ^{13}C labelled BlaC-inhibitor
214 samples to confirm the assignments.
215

216 **Avibactam.**

217 Avibactam was titrated into a BlaC sample and ^{1}H-^{15}N TROSY-HSQCs were recorded at various
218 avibactam concentrations, showing chemical shift perturbations of the BlaC backbone amide resonances
219 in the slow exchange regime. Lineshapes for the resonances of six amides were fitted with a two-state
220 binding model using TITAN software,(45) yielding upper limits for the apparent K_D and k_{off} of 10 µM

and 10 s^{-1}, respectively (Figure S2). This apparent k_{off} is in line with the 1×10^{-2} s^{-1} found by Soroka *et al.*,(32) while the apparent K_D indicates that the low efficacy of BlaC inhibition by avibactam is caused by the very slow on-rate rather than by low affinity. Interestingly, several peaks that are visible in the spectrum of resting state BlaC broaden beyond detection upon binding with avibactam (Figure 2). These peaks correspond to amides around the binding site, indicating that inhibitor binding induces enhanced chemical exchange broadening in the active site. T_1, T_2 and *NOE* experiments performed at 20 T (Figures S9 and S10) show little change in dynamic behavior relative to the resting state, other than decreased transverse relaxation times around the loop containing Ile105. Like the exchange broadening, this hints at induction of a slow or intermediate exchange process. The unexpectedly high transverse relaxation time and low *NOE* for Val80 were not found in the avibactam-bound state.

CPMG relaxation dispersion measurements at 20 T showed an increased magnitude of the exchange relaxation in the loops of the α domain, around the residues whose resonances broadened beyond detection (Figure 3). The exchange profiles of the individual residues over the pulse frequency are visibly different from those in the free state (Figures 4 and S11), indicating a significantly faster exchange process than the 860 s^{-1} that was found for resting state. A single field global fit of the exchange profiles of 19 backbone amides (Figure S11) yielded an estimate of the active site exchange rate in avibactam-bound state of $(3.4 \pm 0.2) \times 10^3$ s^{-1}. The exchange between free and avibactam-bound BlaC is very slow (<<100 s^{-1}), so the chemical exchange process measured here occurs in the bound state. The enhanced exchange effects are observed around the binding site, particularly in the loops containing Ser130 and Ile105.

Clavulanic acid.

Upon binding with clavulanic acid, like with avibactam, the resonances of several amides around the binding site broaden beyond detection (Figure 2). Moreover, in the clavulanic acid adduct-bound state, at least 21 resonances were found to split into two or more distinct peaks of similar intensity. These

peaks belong to amides around the active site and in the α-domain (Figure 5, magenta and orange spheres). Furthermore, the clavulanic acid adduct-bound state of BlaC is less stable over time than the free and avibactam-bound states. Over the course of days, a gradual appearance of broad background signal in the center of the spectrum was observed, suggesting the formation of molten globule.

The T_1, T_2 and *NOE* of clavulanate-bound BlaC were measured at 20 T (Figures S9 and S10). Average relaxation times (T_1 and T_2, respectively) were found to have shifted from 1.7 s and 45 ms for resting state BlaC to 1.8 s and 40 ms for the adduct, which may be caused by an increase in sample viscosity due to the addition of 100 mM clavulanic acid. Strikingly higher transverse relaxation times were found for several residues in and near loops and terminal regions, as well as for six residues involved in the hydrophobic packing interface between helices 2 and 7 in the α subunit. Moreover, for these residues, the *NOE* is lower than in resting state BlaC. These observations indicate a severe local decrease of internal rigidity upon clavulanic acid inhibition, particularly in loop regions and on the interface between helices 2 and 7.

CPMG relaxation dispersion measurements at 20 T were also performed on clavulanate-bound BlaC. However, most of the resonances that show exchange broadening in the resting state protein were broadened beyond detection in the clavulanate-bound spectra. Moreover, due to the splitting of peaks and the gradual appearance of molten globule-like background signal over time, accurate line shape fitting of the resonances proved impossible in many cases. Residues Glu168 and Asp273 were found to have dispersion profiles with shapes similar to the active site exchange of the resting state protein (e.g. Figure 4, panel *(b)*). Slight elevations in the R_{ex} are observed around the loop containing Ile105, near the base of the Ω-loop and for residue Asp273, but overall the profile of exchange relaxation over all residues, keeping in mind the larger error and the missing data, looks rather similar to that of resting state BlaC (Figure 3). Thus, it seems that the resting state BlaC dynamics are still present upon formation of the clavulanic acid adduct and at the same time additional states are being populated, causing line broadening and peak splitting.

Antimicrobial Agents and Chemotherapy

DISCUSSION

We show that resting state BlaC is mostly rigid on the pico- to nanosecond time scale, similar to the behavior of the other class A β-lactamases for which NMR dynamics studies have been performed, TEM-1(11, 13, 14) and PSE-4.(15) Only Val80 was found to exhibit fast motion, as modelled from the low *NOE* ratios and elevated T_2 relaxation times for its backbone amide. This is surprising, as this amide is located in the long α-helix 2 and the Val80 side chain does not face the outside of the protein but rather the interface between helices 2 and 7.

The BlaC active site exhibits flexibility on the millisecond time scale, as observed by both CPMG relaxation dispersion studies and the broadening beyond detection of several important active site residues (Ser70, Ser130, Thr235 and Thr237). This behavior is also similar to that of other class A β-lactamases,(11–20) and the localization of this chemical exchange in the active site suggests that the dynamics may play a role in catalysis. This can only be the case if the dynamics are as fast as or faster than the maximum catalytic turnover rate of the enzyme. The observed exchange rate of (8.6 ± 0.6) × 10^2 s^{-1} -obtained under the assumption of a two-state exchange model- is faster than the fastest k_{cat} that was reported for BlaC, 111 ± 4 s^{-1} for nitrocefin hydrolysis,(47) which implies that enzyme dynamics may be relevant for catalysis. On the basis of the Bloch-McConnell equations for chemical exchange, it can be shown that at an exchange rate of 860 s^{-1}, the population of the minor state must be sizeable (>15 %) for the resonances of Ser70, Ser130, Thr235 and Thr237 to broaden beyond detection. The chemical shift difference between the major and minor state must be larger than 0.1 ppm for ^{1}H and/or 1 ppm for ^{15}N at 20 T. The link between these four residues is that in every BlaC crystal structure published to date, their respective sidechains each contribute to the hydrogen bonding with either the carboxyl group of a ligand or a phosphate or acetate ion from the buffer. However, upon titration with phosphate, the resonances do not appear,(31) meaning that the binding and dissociation of phosphate cannot explain the chemical exchange broadening of these peaks.

We also report the first dynamics study of a class A β-lactamase dynamics upon inhibitor binding. On the pico-nanosecond time scale the reaction with avibactam stabilizes the Val80 amide, while that with clavulanic acid leads to fast motions for various residues, notably including several that are involved in the hydrophobic packing interface between helices 2 and 7, similar to what was observed for Val80 in resting state BlaC. This result resembles the observation by Stivers *et al.* that several residues of 4-oxalocrotonate tautomerase show a decrease in the order parameter upon inhibitor binding.(48) The authors suggest that the increased flexibility of these residues serves as an entropic contribution to the overall free energy change upon binding, which may well be the same for BlaC. An increase in fast dynamics of backbone amides generally indicates increased flexibility of the peptide bond. Many of the amides for which we observe this phenomenon are on the interface of helices 2 and 7. An increase of backbone flexibility implies reduced stability of the hydrophobic core in that region of the α-domain.

On the millisecond time scale, binding of BlaC to either avibactam or clavulanic acid leads to increased effects of dynamics. In the avibactam-bound state, we observe broadening beyond detection of some peaks and relaxation dispersion of others. All affected amides surround the active site. For the broadening beyond detection to be caused by the ~3400 s^{-1} exchange process identified using CPMG experiments, would require chemical shift differences between the two states that are larger than *ca.* 0.3 ppm for ^{1}H and/or 3 ppm for ^{15}N at 20 T. Alternatively, it is possible that multiple exchange processes take place in the same region of the protein. In any case, the relaxation dispersion results suggest that avibactam binding speeds up the active site exchange process in BlaC significantly.

Inhibition of BlaC with clavulanic acid was likewise accompanied by a broadening of many resonances, in and around the active site of BlaC. These experiments were performed in the presence of a high initial concentration of clavulanic acid, so it cannot be excluded entirely that non-covalent binding of an additional clavulanic acid molecule to the BlaC adduct could cause line broadening. However, an earlier study on such binding to a catalytically inactive mutant of BlaC (S70A) showed

that, if binding occurs at all, the affinity must be very low indeed and line broadening in the BlaC NMR spectrum was not observed.(49) Therefore, we attribute the increased dynamics to the adduct formation.

The chemical environment of all the catalytic residues as well as residues in all the nearby regions appears to be affected by the motions. Interestingly, β-lactam binding was previously reported to also cause increased millisecond dynamics in the active site of an L,D transpeptidase(50) as well as in that of a signal transducer β-lactam sensing domain,(51) suggesting that this behavior might be conserved across a wide range of β-lactam binding proteins.

The question arises how these relatively small adducts, especially the clavulanic acid adduct, which is a mere 70 Da (5 heavy atoms), can have such a major impact on such a broad region of the protein. Sagar *et al*.(52) reported small angle X-ray scattering (SAXS) data yielding an unexpectedly large solvation radius for free BlaC in solution, while BlaC bound to clavulanic acid was found to have a solvation radius closer to that which is expected based on the crystal structure. The authors proposed that free BlaC in solution adopts an 'open' conformation, whereas inhibitor binding locks BlaC in the 'closed' conformation that is observed in all crystal structures so far. If resting state BlaC were indeed to adapt an open conformation in solution, it would likely exhibit a larger rotational correlation time and thus higher transverse and lower longitudinal relaxation times than in the canonical closed conformation. The correlation time measured for the free BlaC on the basis of the relaxation data matched the one calculated from the crystal structure. Binding avibactam did not change the relaxation times much and the sample with clavulanic acid bound even yielded relaxation times indicating an increase of the correlation time. However, the latter was likely caused by an increase in sample viscosity due to the high concentration of the inhibitor. Summarizing, our data provide no evidence for an open state of resting state BlaC. For related β-lactamases, it has been suggested (e.g. (11, 15, 16)) that the process underlying the chemical exchange effects is movement of the tip of the omega-loop into and out of the active site. Such movement could facilitate the flow of solvent and substrate, and aid in positioning of the substrate in the active orientation. If so, the motion would likely affect amides in all

regions that are in contact with the tip of the Ω-loop, such as helix 7 and the loops containing Ser130 and Ile105. This model thus fits well with our data.

To gain more insight into what the various states may look like structurally, we compared bound and unbound β-lactamase crystal structures. Most structures show little variation between bound and unbound forms. In structure 6H2H(49) of BlaC bound to avibactam, however, the Ω-loop was observed in a slightly 'open' conformation, with the C_α atoms of Asn170 and Arg171 positioned ~2 Å further away from the active site than its canonical position, providing further support for the model of Ω-loop movement (Figure 6). Our data suggest the presence of multiple dynamic processes in the bound state. Recently, Olmos *et al.*(53) reported an XFEL study with snapshots at 30, 100, 500 and 2000 ms of the catalytic reaction of ceftriaxone hydrolysis by BlaC. The structures obtained during the reaction show almost no structural variation compared to that of BlaC in the resting state. The only active site residues of which the orientation varies between the structures are Lys73 and Ser130. The Lys73 orientations are similar to those reported by Vandavasi *et al.* for class A β-lactamase Toho-1,(24) except that the non-canonical conformation is oriented towards Ser130, whereas in BlaC it is oriented towards Glu166. One of these conformations allows an extra water molecule to penetrate deep into the active site, between helix 2 (Lys73) and helix 7 (Met135, which is an alanine in BlaC), suggesting a defect of the hydrophobic core such as we observe upon clavulanic acid binding in BlaC. The occupancies of the observed states, 41 and 59 %, respectively, also match the relative occupancies of the doubled peaks of 42 ± 3 % that we observe in our clavulanic acid adduct-bound state spectra. An increasing body of evidence suggests that Lys73 can act as a general base for catalysis (e.g. (24, 54–57)). Langan *et al.* even found that in Toho-1 β-lactamase, Lys73 and several other active site residues alter their conformations in reaction to substrate binding.(58) It therefore seems possible that the chemical exchange we observe upon clavulanic acid binding is related to the interconversion of Lys73 between different conformations (Figure 7). As has been suggested before (e.g. (56, 58, 59)), the Lys73 sidechain may need to be in one conformation for efficient substrate binding and another for efficient product release. Thus, it seems possible that the two conformations observed in crystal structures of Toho-1(24,

57–60) and BlaC,(53) are the cause of the two forms that we observe in the NMR spectra of the BlaC-clavulanic acid adduct. In this way the effects of addition of the small adduct to Ser70 can be transmitted further into and around the active site.

In conclusion, we show that BlaC is highly rigid on the pico-nanosecond time scale, but exhibits flexibility on the millisecond time scale in and around the active site, with an exchange rate of *ca.* 860 s^{-1}. The dynamic behavior of free BlaC is very similar to that of the other class A β-lactamases for which dynamics studies were performed and therefore appears to be conserved amongst class A β-lactamases. We also show that upon inhibition with clavulanic acid, pico-nanosecond stability of the hydrophobic core in the α-domain is disturbed. Moreover, upon binding of either clavulanic acid or avibactam, the prevalence of millisecond dynamics around the active site increases dramatically. In this work we studied the dynamics in BlaC-inhibitor complexes, so the question remains what effect this phenomenon has on the time scale of substrate catalysis. We hypothesized that active site flexibility of β-lactamases represents exchange between respective binding modes for the various substrates. The observation that inhibitor binding does not lock the active site in one conformation but rather increases the dynamics, argues against a model of inhibitor binding through conformational selection. Rather, the induced dynamics may serve to maximize the likelihood of sampling the precise conformation that lowers the hydrolysis transition state energy barrier for this substrate the most.

ASSOCIATED CONTENT

Supporting information

Supplemental material for this article may be found in the enclosed document.

AUTHOR INFORMATION

Corresponding author.

[#] E-mail: m.ubbink@chem.leidenuniv.nl; phone: +31 71 5274628.

ORCID

Wouter Elings: 0000-0003-0304-2874

Hugo van Ingen: 0000-0002-0808-3811

Marcellus Ubbink: 0000-0002-2615-6914

Funding

This study was supported by internal funding and by grant number 723.013.010 from the Netherlands Organization for Scientific Research (NWO).

Notes

The authors declare no competing financial interest.

ACKNOWLEDGEMENTS

We would like to thank dr. Karthick Sai Sankar Gupta and Alfons Lefeber for their assistance with the NMR spectrometers and prof. Lewis Kay for providing the TROSY-CPMG pulse sequence.

REFERENCES

1. Greives N, Zhou H-X. 2014. Both protein dynamics and ligand concentration can shift the binding mechanism between conformational selection and induced fit. Proc Natl Acad Sci U S A 111:10197–10202.
2. Vogt AD, Di Cera E. 2012. Conformational selection or induced fit? A critical appraisal of the kinetic mechanism. Biochemistry 51:5894–5902.
3. Du X, Li Y, Xia Y-L, Ai S-M, Liang J, Sang P, Ji X-L, Liu S-Q. 2016. Insights into Protein-Ligand Interactions: Mechanisms, Models, and Methods. Int J Mol Sci 17.
4. Yon JM, Perahia D, Ghélis C. 1998. Conformational dynamics and enzyme activity. Biochimie 80:33–42.
5. Wand AJ. 2001. Dynamic activation of protein function: A view emerging from NMR spectroscopy. Nat Struct Biol 8:926–931.

418 6. Kay LE. 2005. NMR studies of protein structure and dynamics. J Magn Reson 173:193–207.

419 7. Bhabha G, Lee J, Ekiert DC, Gam J, Wilson IA, Dyson HJ, Benkovic SJ, Wright PE. 2011. A
420 Dynamic Knockout Reveals That Conformational Fluctuations Influence the Chemical Step of
421 Enzyme Catalysis. Science (80-) 332:234–238.

422 8. Kohen A. 2015. Role of Dynamics in Enzyme Catalysis: Substantial versus Semantic
423 Controversies. Acc Chem Res 48:466–473.

424 9. Kovermann M, Rogne P, Wolf-Watz M. 2016. Protein dynamics and function from solution state
425 NMR spectroscopy. Q Rev Biophys.

426 10. Petrović D, Risso VA, Kamerlin SCL, Sanchez-Ruiz JM. 2018. Conformational dynamics and
427 enzyme evolution. J R Soc Interface 15.

428 11. Fisette O, Morin S, Savard P-Y, Lagüe P, Gagné SM. 2010. TEM-1 backbone dynamics-insights
429 from combined molecular dynamics and nuclear magnetic resonance. Biophys J 98:637–645.

430 12. Roccatano D, Sbardella G, Aschi M, Amicosante G, Bossa C, Nola A Di, Mazza F. 2005.
431 Dynamical Aspects of TEM-1 β-Lactamase Probed by Molecular Dynamics. J Comput Aided
432 Mol Des 19:329–340.

433 13. Savard P-Y, Gagné SM. 2006. Backbone dynamics of TEM-1 determined by NMR: Evidence for
434 a highly ordered protein. Biochemistry 45:11414–11424.

435 14. Doucet N, Savard P-Y, Pelletier JN, Gagné SM. 2007. NMR investigation of Tyr105 mutants in
436 TEM-1 beta-lactamase: dynamics are correlated with function. J Biol Chem 282:21448–21459.

437 15. Morin S, Gagné SM. 2009. NMR Dynamics of PSE-4 β-Lactamase: An Interplay of ps-ns Order
438 and μs-ms Motions in the Active Site. Biophys J 96:4681–4691.

439 16. Fisette O, Gagné S, Lagüe P. 2012. Molecular Dynamics of Class A β-lactamases—Effects of
440 Substrate Binding. Biophys J 103:1790–1801.

441 17. Risso VA, Gavira JA, Mejia-Carmona DF, Gaucher EA, Sanchez-Ruiz JM. 2013. Hyperstability
442 and Substrate Promiscuity in Laboratory Resurrections of Precambrian β-Lactamases. J Am
443 Chem Soc 135:2899–2902.

444 18. Zou T, Risso VA, Gavira JA, Sanchez-Ruiz JM, Ozkan SB. 2015. Evolution of Conformational
445 Dynamics Determines the Conversion of a Promiscuous Generalist into a Specialist Enzyme. Mol
446 Biol Evol 32:132–143.
447 19. Risso VA, Martinez-Rodriguez S, Candel AM, Krüger DM, Pantoja-Uceda D, Ortega-Muñoz M,
448 Santoyo-Gonzalez F, Gaucher EA, Kamerlin SCL, Bruix M, Gavira JA, Sanchez-Ruiz JM. 2017.
449 De novo active sites for resurrected Precambrian enzymes. Nat Commun 8:16113.
450 20. Clouthier CM, Morin S, Gobeil SMC, Doucet N, Blanchet J, Nguyen E, Gagné SM, Pelletier JN.
451 2012. Chimeric β-Lactamases: Global Conservation of Parental Function and Fast Time-Scale
452 Dynamics with Increased Slow Motions. PLoS One 7:e52283.
453 21. Gobeil SMC, Clouthier CM, Park J, Gagné D, Berghuis AM, Doucet N, Pelletier JN. 2014.
454 Maintenance of Native-like Protein Dynamics May Not Be Required for Engineering Functional
455 Proteins. Chem Biol 21:1330–1340.
456 22. González MM, Abriata LA, Tomatis PE, Vila AJ. 2016. Optimization of Conformational
457 Dynamics in an Epistatic Evolutionary Trajectory. Mol Biol Evol 33:1768–1776.
458 23. Meroueh SO, Fisher JF, Schlegel HB, Mobashery S. 2005. Ab Initio QM/MM Study of Class A
459 β-Lactamase Acylation: Dual Participation of Glu166 and Lys73 in a Concerted Base Promotion
460 of Ser70. J Am Chem Soc 127:15397–15407.
461 24. Vandavasi VG, Weiss KL, Cooper JB, Erskine PT, Tomanicek SJ, Ostermann A, Schrader TE,
462 Ginell SL, Coates L. 2016. Exploring the Mechanism of β-Lactam Ring Protonation in the Class
463 A β-lactamase Acylation Mechanism Using Neutron and X-ray Crystallography. J Med Chem
464 59:474–479.
465 25. Drawz SM, Bonomo RA. 2010. Three decades of β-lactamase inhibitors. Clin Microbiol Rev
466 23:160–201.
467 26. Papp-Wallace KM, Bonomo RA. 2016. New β-lactamase inhibitors in the clinic. Infect Dis Clin
468 North Am 30:441–464.
469 27. Tehrani KHME, Martin NI. 2018. β-lactam/β-lactamase inhibitor combinations: an update.

Medchemcomm 9:1439–1456.

28. Kurz SG, Bonomo RA. 2012. Reappraising the use of β-lactams to treat tuberculosis. Expert Rev Anti Infect Ther 10:999–1006.

29. Watkins RR, Papp-Wallace KM, Drawz SM, Bonomo RA. 2013. Novel β-lactamase inhibitors: a therapeutic hope against the scourge of multidrug resistance. Front Microbiol 4:392.

30. Drawz SM, Papp-Wallace KM, Bonomo RA. 2014. New β-Lactamase Inhibitors: a Therapeutic Renaissance in an MDR World. Antimicrob Agents Chemother 58:1835–1846.

31. Elings W, Tassoni R, van der Schoot SA, Luu W, Kynast JP, Dai L, Blok AJ, Timmer M, Florea BI, Pannu NS, Ubbink M. 2017. Phosphate promotes the recovery of *Mycobacterium tuberculosis* β-lactamase from clavulanic acid inhibition. Biochemistry 56:6257–6267.

32. Soroka D, Ourghanlian C, Compain F, Fichini M, Dubée V, Mainardi JL, Hugonnet JE, Arthur M. 2017. Inhibition of β-lactamases of mycobacteria by avibactam and clavulanate. J Antimicrob Chemother 72:1081–1088.

33. Ambler RP, Coulson AFW. 1991. A standard numbering scheme for the Class A beta-lactamases. Biochem J 276:269–272.

34. Pervushin K, Riek R, Wider G, Wüthrich K. 1997. Attenuated T2 relaxation by mutual cancellation of dipole-dipole coupling and chemical shift anisotropy indicates an avenue to NMR structures of very large biological macromolecules in solution. Proc Natl Acad Sci U S A 94:12366–12371.

35. Schanda P, Van Melckebeke H, Brutscher B. 2006. Speeding up three-dimensional protein NMR experiments to a few minutes. J Am Chem Soc 128:9042–9043.

36. Vranken WF, Boucher W, Stevens TJ, Fogh RH, Pajon A, Llinas M, Ulrich EL, Markley JL, Ionides J, Laue ED. 2005. The CCPN data model for NMR spectroscopy: Development of a software pipeline. Proteins: Struct, Funct, Bioinf 59:687–696.

37. Bae S-H, Dyson HJ, Wright PE. 2009. Prediction of the rotational tumbling time for proteins with disordered segments. J Am Chem Soc 131:6814–6821.

496 38. García de la Torre J, Huertas M., Carrasco B. 2000. HYDRONMR: Prediction of NMR
497 Relaxation of Globular Proteins from Atomic-Level Structures and Hydrodynamic Calculations. J
498 Magn Reson 147:138–146.
499 39. Bruker Corporation. 2018. Dynamics Center Manual 003:110.
500 40. Woessner DE. 1962. Nuclear Spin Relaxation in Ellipsoids Undergoing Rotational Brownian
501 Motion. J Chem Phys 37:647–654.
502 41. Vallurupalli P, Hansen DF, Stollar E, Meirovitch E, Kay LE. 2007. Measurement of bond vector
503 orientations in invisible excited states of proteins. Proc Natl Acad Sci U S A 104:18473–18477.
504 42. Delaglio F, Grzesiek S, Vuister G, Zhu G, Pfeifer J, Bax A. 1995. NMRPipe: A multidimensional
505 spectral processing system based on UNIX pipes. J Biomol NMR 6:277–293.
506 43. Hansen DF, Yang D, Feng H, Zhou Z, Wiesner S, Bai Y, Kay LE. 2007. An exchange-free
507 measure of 15 N transverse relaxation: An NMR spectroscopy application to the study of a
508 folding intermediate with pervasive chemical exchange. J Am Chem Soc 129:11468–11479.
509 44. Hansen DF, Vallurupalli P, Lundström P, Neudecker P, Kay LE. 2008. Probing chemical shifts of
510 invisible states of proteins with relaxation dispersion NMR spectroscopy: How well can we do? J
511 Am Chem Soc 130:2667–2675.
512 45. Waudby CA, Ramos A, Cabrita LD, Christodoulou J. 2016. Two-Dimensional NMR Lineshape
513 Analysis. Sci Rep 6:24826.
514 46. Xu H, Hazra S, Blanchard JS. 2012. NXL104 irreversibly inhibits the β-lactamase from
515 *Mycobacterium tuberculosis*. Biochemistry 51:4551–4557.
516 47. Hugonnet J-E, Blanchard JS. 2007. Irreversible inhibition of the *Mycobacterium tuberculosis*
517 beta-lactamase by clavulanate. Biochemistry 46:11998–12004.
518 48. Stivers JT, Abeygunawardana C, Mildvan AS, Whitman CP. 1996. 15 N NMR Relaxation
519 Studies of Free and Inhibitor-Bound 4-Oxalocrotonate Tautomerase: Backbone Dynamics and
520 Entropy Changes of an Enzyme upon Inhibitor Binding. Biochemistry 35:16036–16047.
521 49. Tassoni R, Blok A, Pannu NS, Ubbink M. 2019. New Conformations of Acylation Adducts of

Inhibitors of β-Lactamase from Mycobacterium tuberculosis. Biochemistry 58:997–1009.

50. Lecoq L, Bougault C, Hugonnet JE, Veckerlé C, Pessey O, Arthur M, Simorre JP. 2012. Dynamics induced by β-lactam antibiotics in the active site of Bacillus subtilis l,d-transpeptidase. Structure 20:850–861.

51. Frederick TE, Peng JW. 2018. A gratuitous β-Lactamase inducer uncovers hidden active site dynamics of the Staphylococcus aureus BlaR1 sensor domain. PLoS One 13:e0197241.

52. Sagar A, Haleem N, Bashir YM, Ashish. 2017. Search for non-lactam inhibitors of mtb β-lactamase led to its open shape in apo state: new concept for antibiotic design. Sci Rep 7:6204.

53. Olmos JL, Pandey S, Martin-Garcia JM, Calvey G, Katz A, Knoska J, Kupitz C, Hunter MS, Liang M, Oberthuer D, Yefanov O, Wiedorn M, Heyman M, Holl M, Pande K, Barty A, Miller MD, Stern S, Roy-Chowdhury S, Coe J, Nagaratnam N, Zook J, Verburgt J, Norwood T, Poudyal I, Xu D, Koglin J, Seaberg MH, Zhao Y, Bajt S, Grant T, Mariani V, Nelson G, Subramanian G, Bae E, Fromme R, Fung R, Schwander P, Frank M, White TA, Weierstall U, Zatsepin N, Spence J, Fromme P, Chapman HN, Pollack L, Tremblay L, Ourmazd A, Phillips GN, Schmidt M. 2018. Enzyme intermediates captured “on the fly” by mix-and-inject serial crystallography. BMC Biol 16:59.

54. Golemi-Kotra D, Meroueh SO, Kim C, Vakulenko SB, Bulychev A, Stemmler AJ, Stemmler TL, Mobashery S. 2004. The importance of a critical protonation state and the fate of the catalytic steps in class A beta-lactamases and penicillin-binding proteins. J Biol Chem 279:34665–34673.

55. Nichols DA, Hargis JC, Sanishvili R, Jaishankar P, Defrees K, Smith EW, Wang KK, Prati F, Renslo AR, Woodcock HL, Chen Y. 2015. Ligand-Induced Proton Transfer and Low-Barrier Hydrogen Bond Revealed by X-ray Crystallography. J Am Chem Soc 137:8086–8095.

56. Pan X, He Y, Lei J, Huang X, Zhao Y. 2017. Crystallographic snapshots of Class A β-lactamase catalysis reveal structural changes that facilitate β-lactam hydrolysis. J Biol Chem 4022–4033.

57. Vandavasi VG, Langan PS, Weiss KL, Parks JM, Cooper JB, Ginell SL, Coates L. 2017. Active-Site Protonation States in an Acyl-Enzyme Intermediate of a Class A β-Lactamase with a

548 Monobactam Substrate. Antimicrob Agents Chemother 61.
549 58. Langan PS, Vandavasi VG, Cooper SJ, Weiss KL, Ginell SL, Parks JM, Coates L. 2018.
550 Substrate Binding Induces Conformational Changes in a Class A β-lactamase That Prime It for
551 Catalysis. ACS Catal 8:2428–2437.
552 59. Tomanicek SJ, Blakeley MP, Cooper J, Chen Y, Afonine P V., Coates L. 2010. Neutron
553 Diffraction Studies of a Class A β-Lactamase Toho-1 E166A/R274N/R276N Triple Mutant. J
554 Mol Biol 396:1070–1080.
555 60. Ibuka AS, Ishii Y, Galleni M, Ishiguro M, Yamaguch K, Frère J-M, Matsuzawa H, Sakai H.
556 2003. Crystal Structure of Extended-Spectrum β-Lactamase Toho-1: Insights into the Molecular
557 Mechanism for Catalytic Reaction and Substrate Specificity Expansion.
558 61. Tremblay LW, Hugonnet J-E, Blanchard JS. 2008. Structure of the covalent adduct formed
559 between *Mycobacterium tuberculosis* beta-lactamase and clavulanate. Biochemistry 47:5312–
560 5316.

561 **FIGURES**

562 Figure 1. Crystal structure of BlaC (subunit A of PDB entry code 5NJ2).(31) *(a)* Cartoon representation
563 with indication of α-helices, β-strands and the Ω-loop. Several active site residues are shown in stick
564 representation. *(b)* Detail of the active site, showing both stick representation and transparent cartoon
565 representation for clarity. Several active site residues and the conserved active site water molecule are
566 indicated.

567

568 Figure 2. Peak intensities. *(a)* Relative peak intensities of assigned backbone amides in a $^{1}H,^{15}N$ TROSY
569 spectrum, for BlaC in resting state (black squares), bound to clavulanic acid (red circles), and bound to
570 avibactam (blue triangles). The resonance of the C-terminal amide was used for normalization. The
571 break on the horizontal axis represents a BlaC-specific G-G-G-T-loop which is not present in the
572 Ambler numbering. Several active site residues are indicated with grey bars. Secondary structure is

indicated above the graph, light and dark grey boxes represent α-helices and β-strands, respectively. Error bars have been omitted for clarity, propagated error from the spectral noise is in all cases <0.03. *(b)-(c)* Visualization of binding effects on BlaC crystal structure with PDB entry code 5NJ2. Non-proline backbone amides for which no resonance was found in free BlaC are indicated with red spheres. Amides for which the resonance was lost upon inhibitor binding are indicated with orange spheres for clavulanic acid *(b)* and avibactam *(c)*. Amides for which a resonance could be assigned for resting state as well as bound BlaC are indicated with blue spheres. Proline nitrogen atoms are indicated with black spheres. Amides of several active site residues are indicated for reference.

Figure 3. CPMG relaxation dispersion data. *(a)* Contribution of chemical exchange to the R_2 relaxation of backbone ^{15}N resonances in BlaC resting state (black), bound to clavulanic acid (red) and bound to avibactam (blue), as measured by CPMG relaxation dispersion analysis at 20 T. R_{ex} is defined as the $R_{2,eff}$ at ν_{CPMG} = 25 s^{-1} minus that at 1000 s^{-1}. Error bars represent the 95% confidence interval based on three duplicate delays per experiment. The break on the horizontal axis represents a BlaC-specific G-G-G-T-loop which is not present in the Ambler numbering. Several active site residues are indicated with grey bars. Secondary structure is indicated above the graph; light and dark grey boxes represent α-helices and β-strands, respectively. *(b)-(d)* Visualization of millisecond dynamics on BlaC structure 5NJ2,(31) for BlaC bound to clavulanic acid *(b)*, in free state *(c)* and bound to avibactam *(d)*. Backbone amides for which R_{ex} < 3 s^{-1} are displayed as blue spheres, those with R_{ex} > 3 s^{-1} as orange spheres. Residues whose resonances were broadened beyond detection are displayed as red spheres, while those for which R_{ex} could not be determined for another reason (e.g. prolines or too much peak overlap) are displayed as black spheres.

Figure 4. Example CPMG relaxation dispersion profiles, as measured at 20 T. Data obtained in the free state, bound to clavulanic acid adduct and bound to avibactam are represented in black squares, red

598 circles and blue triangles, respectively. Error bars represent the standard deviation based on three
599 duplicate CPMG frequencies, with a user-defined minimum of 0.8 s^{-1} to avoid overfitting. Lines
600 represent global fits to a two-state exchange model as described in the text.

601

602 Figure 5. Dynamics of BlaC upon reaction with clavulanic acid. Backbone amides for which the
603 resonance has broadened beyond detection are displayed in red, those for which multiple resonances
604 could be assigned in magenta, those for which a transverse relaxation time T_2 > 60 ms was found in
605 cyan, those for which the cyan and magenta conditions are both true in orange and those for which no
606 severe dynamics were detected in blue. Proline nitrogen atoms are displayed in black.

607

608 Figure 6. Ω-loop displacement model. Cartoon representation of the BlaC active site in an alignment of
609 BlaC crystal structures in free form (5NJ2 and 5OYO(31)) in green, bound to clavulanic acid adduct
610 (3CG5,(61) 6H2C and 6H2G(49)) in yellow and bound to avibactam (4DF6(46) and 6H2H(49)) in
611 orange. Active site residues Ser70 and Glu166 are shown in stick representation, adducts are omitted for
612 clarity. Structure 6H2H of BlaC bound to avibactam displays a more 'open' conformation of the Ω-loop.

613

614 Figure 7. Alternative model involving reorientation of Lys73. BlaC structures observed by Olmos *et al.*,
615 representing bound (PDB 5A92, green carbons) and unbound states (PDB 5A91, yellow carbons), show
616 different orientations for the sidechain of Lys73.(53) Indicated distances are in Ångström.

617

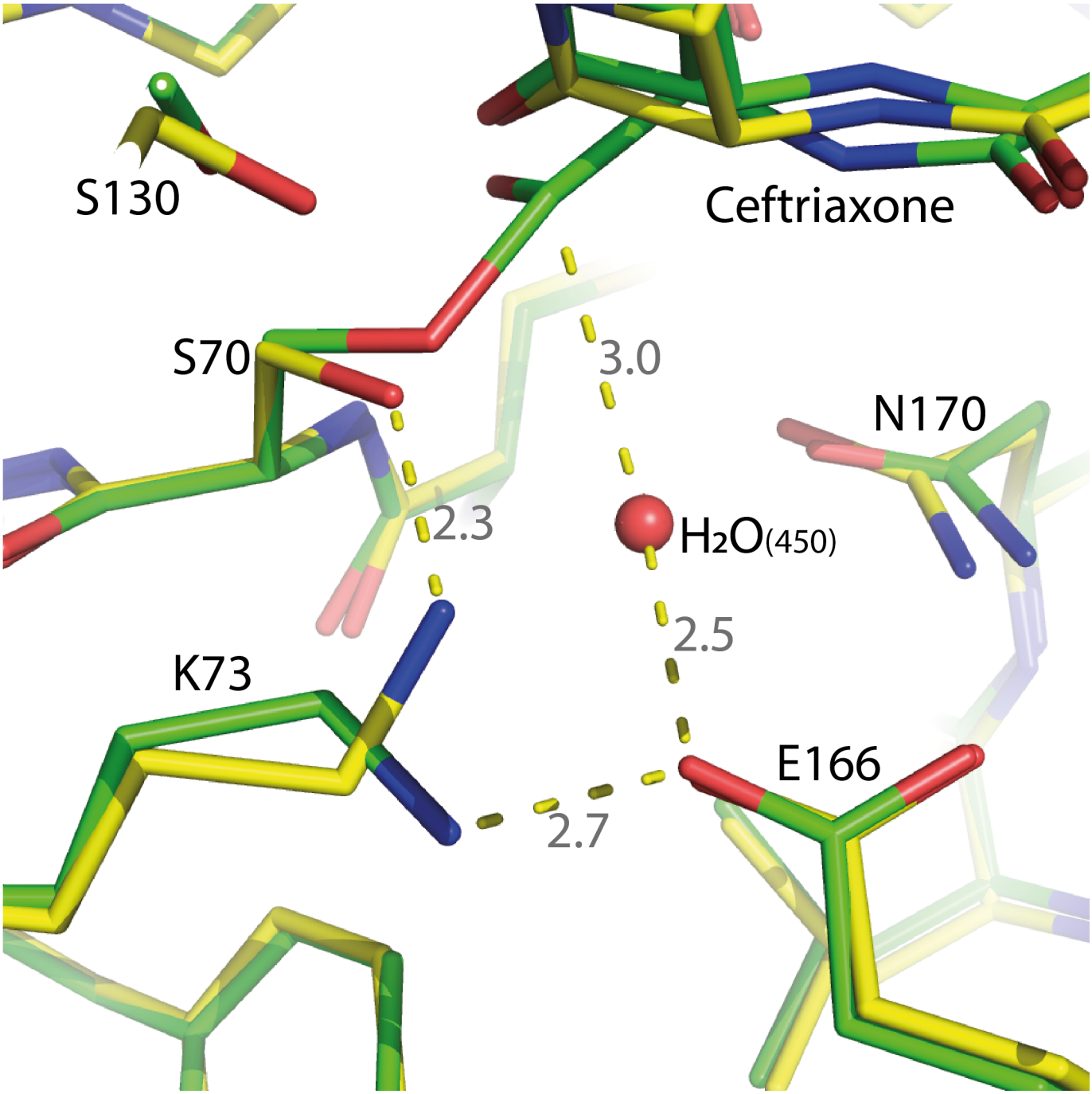

Antimicrobial Agents and Chemotherapy

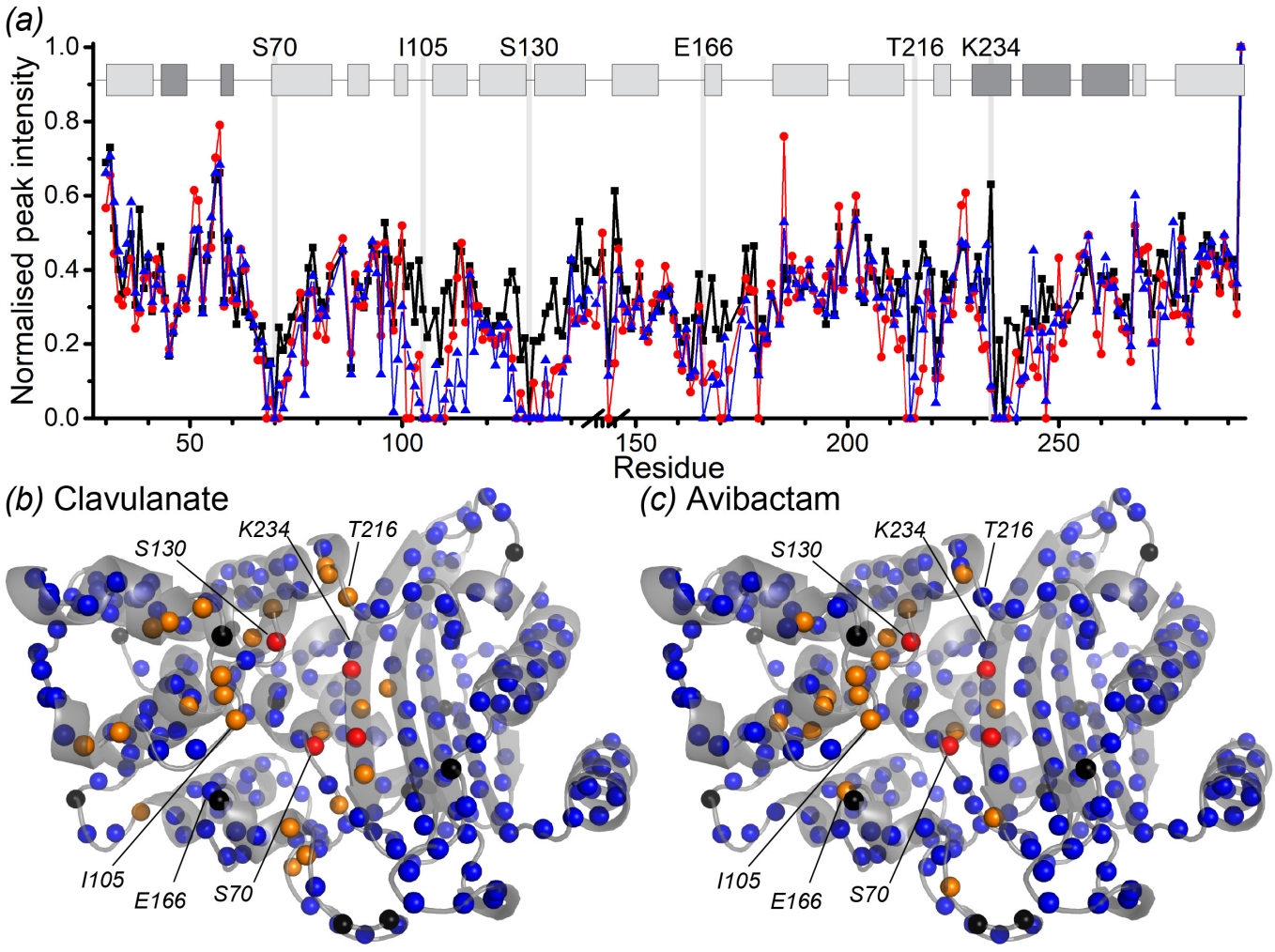

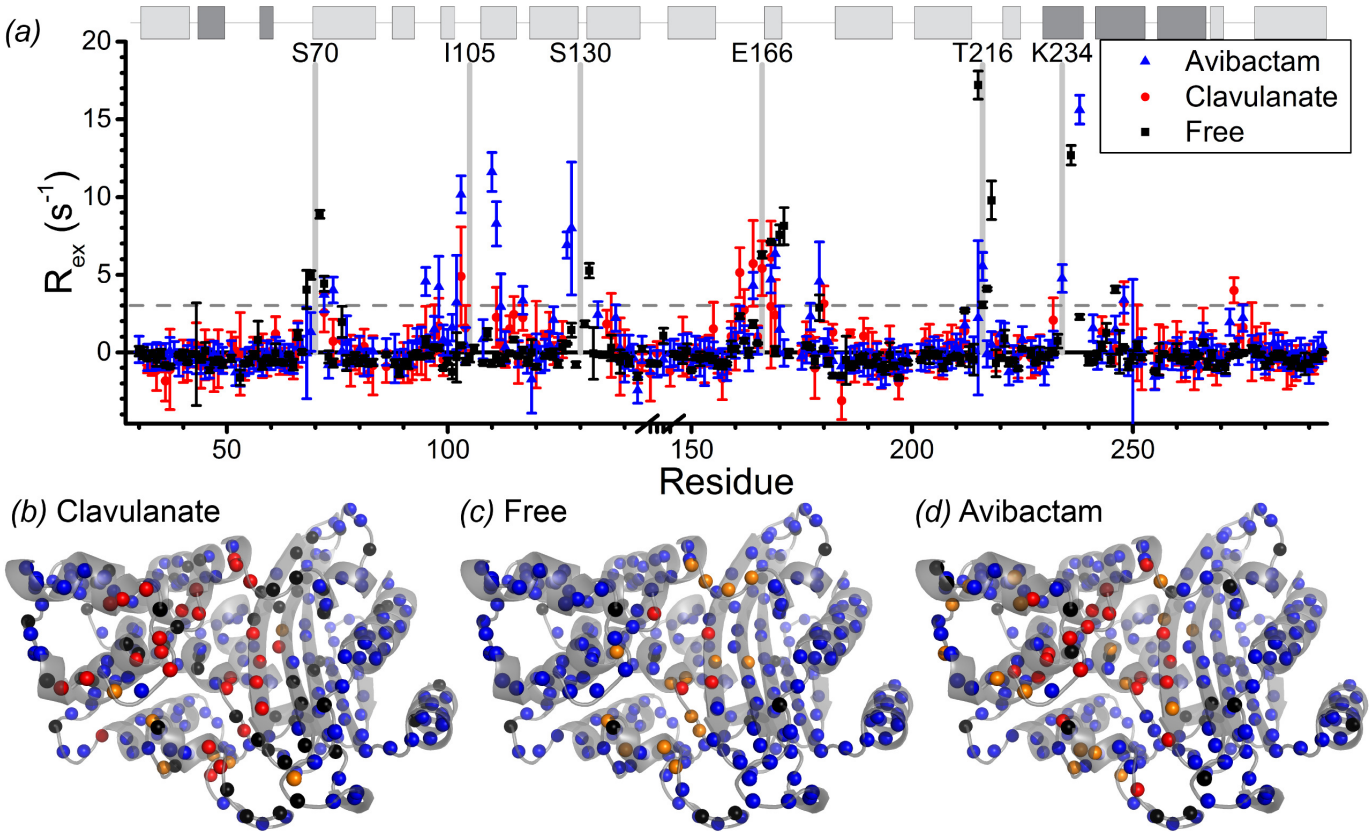

Antimicrobial Agents and Chemotherapy